Novel optical fiber-based laser direct writing process for micromachining of metal

Kwang H. Oh[1*], S. S. Woo[1], H. S. Jeong[1], Y. W. Yi[1], and S. H. Jeong[2]

[1] *Laser Advanced System Industrialization Center (LASIC) Jeonnam Technopark, Stiftung, 200, Yeongcheon, Jangseong-Eup, Jangseong-Gun, Jeollanam-Do, 515-806, Republic of Korea*

[2] *School of Mechatronics, Gwangju Institute of Science and Technology, 123, Cheomdan-Gwagiro, Buk-Gu, Gwangju Megalopolis, 500-712, Republic of Korea*

[*] *Corresponding author: sharkie@jntp.or.kr*

Received March 20, 2012; accepted August 13, 2012; posted online November, 2012

A laser micromachining technique for the fabrication of metallic microstructures is proposed. The fabrication of microstructures is done by laser-induced wet etching that adopts an optical fiber as a machining tool. The laser beam delivered through the multimode fiber directly irradiates on the workpiece while maintaining a proper gap to avoid fiber damage. The manufacture of microstructures with high surface quality and good size uniformity is realized. Microgrooves with aspect ratio over 10 and microholes with a nearly straight cross-section can be produced by the proposed technique. The overall etching results are examined closely with respect to process variables.

OCIS codes: 140.0140, 140.3390.

doi: 10.3788/COL201210.S21407.

Laser precision microfabrication technology has been frequently adopted for the manufacture of microstructures on a variety of materials in the past decades. The laser material processing in association with a direct writing technique enables to easily provide a rapid prototype of microstructures with no mask or additional processes. Laser-based micromachining of metals has often been achieved with high intensity pulsed laser irradiation[1,2]. However, a large heat affected zone (HAZ) with redeposition of evaporated or resolidificated material and mechanical load on the processed area can have a negative effect on the functional properties of microstructures[3].

As a possible approach to realize material removal while avoiding such issues, laser-induced thermochemical wet etching (LIWE) may be employed. In LIWE, the workpiece is immersed in a liquid etchant that helps the fabrication of microstructures with almost no melting or debris due to cooling effects. The micromachining of workpiece in LIWE is done through thermochemical reaction between the etchant and the workpiece while the laser beam irradiates on the workpiece to locally raise surface temperature. A relatively simple setup compared with picosecond or sub-picosecond pulsed laser machining system is required for LIWE at a substantially lower equipment or maintenance cost. Due to these advantages of LIWE, the fabrication of microstructures using LIWE technique has been studied for various applications. Nowak *et al.*[4,5] fabricated microstructures using LIWE with titanium and stainless steel in phosphoric acid and sulfuric acid, respectively. In the previous research, we also manufactured high-aspect-ratio microgrooves using LIWE and the metallic grooves were adopted for the fabrication of a flat stainless steel micro heat pipe[6]. Recently, the capability of LIWE technique for the manufacture of optically transparent material as well as metals and semiconductors has been demonstrated for the fabrication of photonic devices[7,8].

In spite of these advantages of LIWE, it still suffers from the problem of low throughput due to the use of a single objective lens, which is the intrinsic difficulty of most lens-based laser machining processes. Since a multiple laser beam can be a solution to this issue, many researches have been conducted for the use of diffractive optical elements. For instance, Hasegawa *et al.*[9] reported that the feasibility of holographic parallel laser processing of arbitrary three-dimensional (3D) structures with a single laser pulse using a phase Fresnel lens. In this case, however, a complicated beam alignment was required and other optical element such as a spatial modulator to obtain uniform intensity was inevitable. For the practical application of a laser micromachining technique, including LIWE, it is desired to be able to increase throughput with little alignment difficulty or loss of laser beam power.

In this letter, a novel optical fiber-based LIWE method to fabricate microstructures with good surface quality and size uniformity is introduced. Optical fiber plays a central role as a light waveguide and machining tool in the proposed new LIWE setup. The laser beam is delivered through an optical fiber and instead of using an objective lens the fiber tip is directly brought to the surface of a workpiece to irradiate and micromachine the workpiece. Since the laser beam is delivered through the optical fiber, the risk of exposure of an operator to high power laser light is completely eliminated. Throughput enhancement by multiplexing of the laser beam using an optical splitter is also discussed. The fabrication characteristics of microgrooves and microholes in stainless steel utilizing the proposed LIWE technique are closely investigated for varying process conditions.

A schematic diagram of the experimental setup for the optical fiber-based LIWE system to fabricate metallic microstructures is shown in Fig. 1. A Q-switch pulsed Nd:YAG laser (λ_o= 532 nm, P_{max}= 60 W, τ=5 ns, P_{rr}= 10 kHz, TEM_{00}) and a DPSS continuous wave (CW) Nd:YVO_4 laser (λ_o= 532 nm, P_{max}= 8 W, TEM_{00},

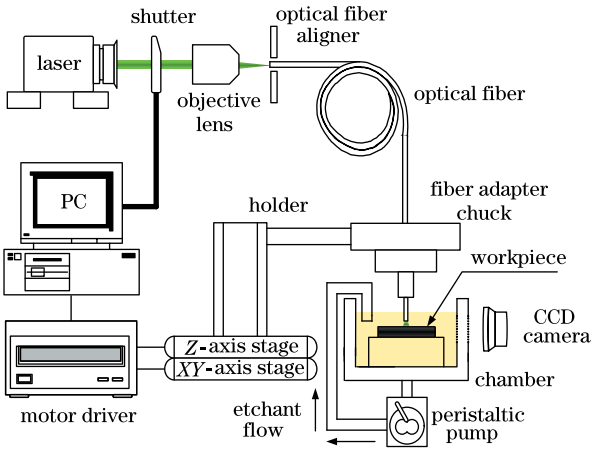

Fig. 1. Schematic diagram of the proposed LIWE setup adopting an optical fiber as the light waveguide and machining tool.

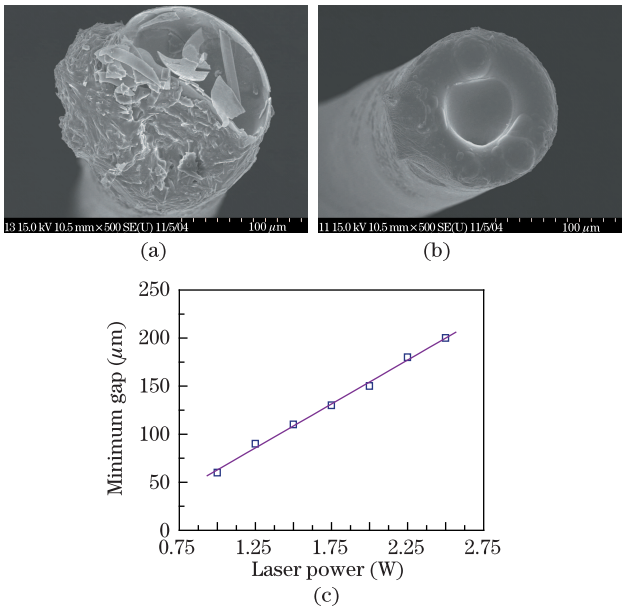

Fig. 2. SEM images for the cross-sectional profile of the (a) fractured and (b) melted fiber due to the generated bubble trapping and (c) the minimum gap required between the fiber tip and the workpiece to prevent fiber damage.

$M^2 < 1.1$) are used as the heat sources for fabricating microgrooves and microholes, respectively. The output laser beam was focused by using an objective lens (5×, FL=40 mm, WD=37.5 mm, NA=0.14, DOF=14 μm) to effectively launch into the optical fibers. Commercially available multimode fibers with core diameters of 50 and 105 μm (D_{clad}=125 μm, NA=0.22) were used as the light waveguide to deliver high power laser beam and direct machining tool. To circulate etchant continuously, a peristaltic pump was used. The fiber is installed on a high resolution (1 μm/pulse) motorized X-Y-Z stage for direct writing. A stainless steel foil (Fe72/Cr18/Ni10, 500-μm thickness) of 1×2 (cm) area is used as the workpiece to study etching process. Phosphoric acid (H_3PO_4, 85%) diluted with distilled water are used as the etchant. All etching processes are monitored in real time with a charge-coupled device (CCD) camera and etching results are examined using an optical microscope and scanning electron microscope (SEM).

To perform LIWE using the proposed technique, the gap between fiber tip and workpiece surface should be well controlled. Otherwise, damage of the fiber tip will easily occur. Figures 2(a) and (b) show SEM images of the damaged fiber tips. Bubble generation is indispensable during wet etching[10]. Once a bubble is trapped between the fiber tip and workpiece, a vapor layer is formed and the fiber tip becomes seriously damaged in the form of fracture or melting due to concentrated laser beam. Another cause of the damage is possibly due to the direct contact of the fiber tip to workpiece surface. In our repeated experiments, the number of bubbles greatly increased and their sizes tended to be bigger at the damage condition. The bubble generation during etching is much more active at higher laser power or narrower gap, resulting in fiber damage. In order to reduce damage of the fiber tip due to the bubble trap, a certain gap was maintained constantly while the workpiece is etched. Figure 2(c) represents the experimentally verified minimum gap, D_{gap}, that should be guaranteed between the workpiece and fiber tip for LIWE to avoid fiber damage.

The surface of austenitic stainless steel is protected by a native thin chromium oxide layer that nearly prohibits the progress of etching in the etchant (H_3PO_4) under room temperature. However, when heat is supplied to the workpiece by laser irradiation raising the surface temperature above an etch threshold, thermally activated chemical reaction occurs and a local removal of the passivation layer is started[11]. In general, the chemical reaction between stainless steel and H_3PO_4 is very complex to analyze because the detailed reaction channels of iron, chromium, and nickel elements in stainless steel are not clearly known. Chromium oxide (Cr_2O_3) passivation layer natively formed on the surface of stainless steel, however, is removed through thermochemical reaction upon laser irradiation, generating soluble chromium orthophosphate ($CrPO_4$) and H_2O as by-products[12]. A possible reaction equation could be expressed as $Cr_2O_3+2H_3PO_4 \rightarrow 2CrPO_4+3H_2O$. Under the region where the passivation layer is eliminated, the reactions of iron, chromium, and nickel with the etchant are expected to occur through several possible reaction channels. Almeida *et al.*[13] studied the chemical reaction of stainless steels in phosphoric acid with various concentrations for a long exposure time. The authors demonstrated that iron chemically reacts with H_3PO_4 to produce soluble ferrous phosphate ($Fe_3(PO_4)_2$) as a by-product. In an electrochemical test of corrosion behavior of stainless steel, Iken *et al.*[14] suggested the formation of Fe, Cr, and Ni oxides through a reaction with water molecules and also reported that the corrosion rate increased for increasing temperature.

Referring to these studies, it is considered that the etching of stainless steel occurs through the dissolution of metal elements in H_3PO_4 to form soluble phosphates such as $Fe_3(PO_4)_2$, $CrPO_4$, etc. To verify the dissolution of iron, chromium, and nickel in H_3PO_4 during etching, the used etchant after an etching experiment was analyzed using an inductively coupled plasma (ICP)-mass spectrometer and the results are shown in Table 1.

Table 1. ICP-Mass Spectroscopy Data of the H_3PO_4 Solution Used for Etching

Element	Mass	CPS	Concentration
Cr	52	11 609.62 P	3.594 ppm
Fe	57	898.950 7 P	14.73 ppm
Ni	60	2 400.284 P	1.435 ppm

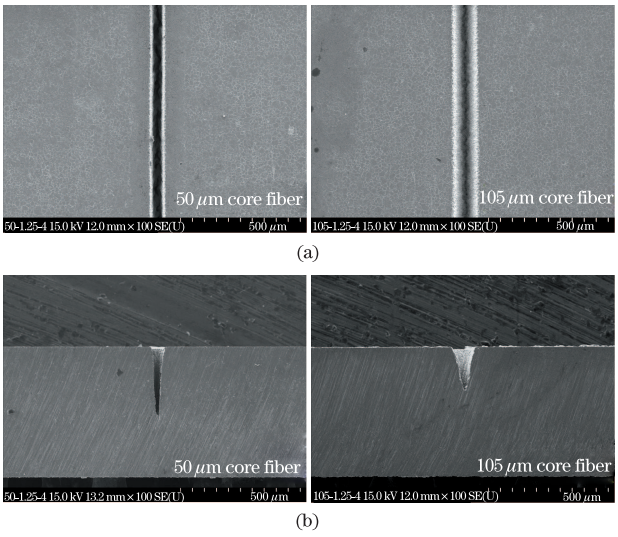

Fig. 3. SEM images for the (a) surface morphologies and (b) cross-sectional profiles of stainless steel microgrooves fabricated in 10% H_3PO_4 with two different core fibers. Other process parameters are P=1.25 W, V=4 μm/s, and $D_{\rm gap}$=90 μm.

Although the information for individual soluble compounds is not available, it can be seen that the ratio of metallic elements in the used etchant is almost the same as the original composition of the bulk sample, implying that overall etching of the metal, not elementally selective etching, takes place during LIWE process.

The characteristics of microstructures fabricated using LIWE depend significantly upon the process variables such as laser power (P), scan speed (V), etchant concentration (C), core diameter of the optical fiber ($D_{\rm core}$), and the gap ($D_{\rm gap}$) between fiber tip and workpiece surface. Accordingly, to fabricate microstructures with good shape and size accuracy using the proposed LIWE technique, the process conditions should be well adjusted.

Figure 3 shows the surface morphology and cross-sectional profile of the microgrooves produced using optical fibers with two different core diameters, 50 and 105 μm. 'Single laser irradiation' instead of multiple scanning as was in our earlier study[6] is done in 10% H_3PO_4 with the process conditions of P=1.25 W, V=4 μm/s, $D_{\rm gap}$=100 μm. The observed difference in groove widths at the top surface in Fig. 3(a) is obviously due to the difference in core diameter between the optical fibers. Regardless of the core size, the surfaces have high shape clarity and no evidence of melting or debris formation. The measured full-width at half-maximum (FWHM) depths of the grooves fabricated with 50- and 105-μm-core fibers are 27 and 43 μm, respectively. The cross-sectional profiles in Fig. 3(b) show significantly different characteristics. Although numerical apertures of the two fibers are exactly the same at the value of 0.22, laser power density of the 50-μm-core fiber is around 4 times greater than that of 105-μm-core fiber resulting in the fabrication of a deeper and narrower groove. The depths of microgrooves for 50-μm- and 105-μm-core fibers are about 290 and 175 μm for which the corresponding aspect ratios defined by 'depth/FWHM' are 10.7 and 4.1, respectively. These results verify that the manufacture of a narrow and deep microgroove is possible using a normal fiber with no focusing components and demonstrate that the proposed LIWE is an useful micromachining technique to fabricate high-aspect-ratio microgrooves. Experiments for the fabrication of microgrooves are conducted at various laser powers and scan speeds and the results showed that top width and surface quality remain basically the same as those in Fig. 3(a). Although the shapes of cross-section of the grooves are similar to those in Fig. 3(b), actual depth of the grooves increases substantially for smaller core diameter and increasing laser power. The maximum aspect ratio achieved in the present study is about 14 with groove width and depth of 32 and 457 μm, respectively, for which the process conditions are P=2 W, V=2 μm/s, $D_{\rm gap}$=150 μm, and $D_{\rm core}$=50 μm, in 10% H_3PO_4.

In our previous research, we have ever fabricated stainless steel microgrooves with an aspect ratio over 10 using conventional lens-based LIWE technique with a CW laser[6]. The microgrooves had good size uniformity and high surface quality and they were by no means inferior to those fabricated by the present optical fiber-based method. Nevertheless, the repeated scan in lens-based technique for the fabrication of a high-aspect-ratio structure led to long process time, resulting in low productivity. Also, the laser beam should be aligned through multiple optics and focused precisely at the workpiece surface, which made the beam alignment become a time consuming problem.

The optical-fiber based method proposed in this work could solve above issues. Figure 4 represents the variations of the etch width, depth, and aspect ratio of the grooves manufactured in 10% H_3PO_4 with the lens-based method and the proposed method while the scan speed is kept at the same value of 10 μm/s. As shown in Fig. 4, size characteristics of the grooves are very close to each other with respect to the variation of the laser power. However, note that the aspect ratio of grooves achieved by single laser scan using the optical fiber-based LIWE technique is as large as that obtained by five repeated scans using the lens-based LIWE. Thanks to the pulsed laser beam with high peak intensity, the fabrication time of a groove could be reduced remarkably. In addition, the alignment difficulty can be removed substantially because maintaining the gap between fiber tip and workpiece is the only alignment requirement in the proposed LIWE system.

One of the most important advantages of the proposed optical fiber-based laser micromachining technique is the potential to enhance manufacturing throughput. Since the laser beam is transmitted through an optical fiber, it is easy to divide the laser beam into multiple beams if a multiplexing element such as an optical splitter is coupled to the emitting end of the optical fiber. Provided that the laser source produces sufficiently high power,

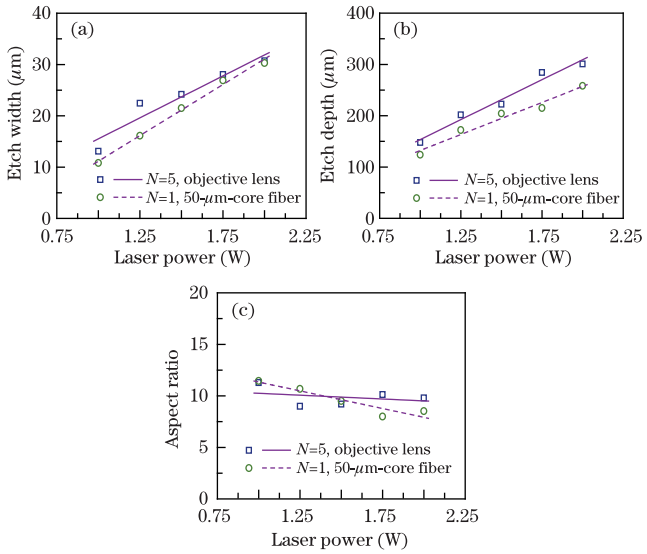

Fig. 4. Variations of the etch (a) width, (b) depth, and (c) aspect ratio of the microgroove fabricated in 10% H_3PO_4 with two different LIWE techniques. The scan speed is kept the same value at V=10 μm/s.

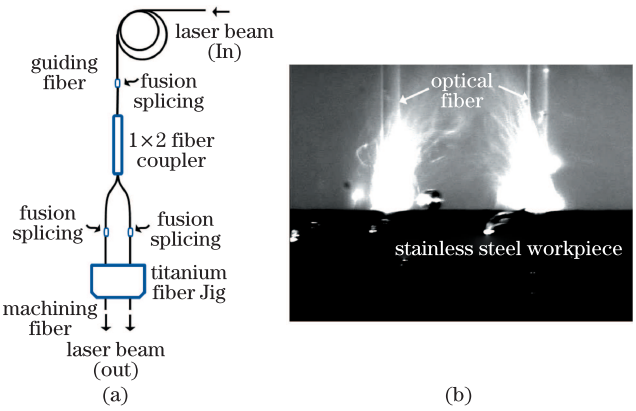

Fig. 5. (a) Schematic diagram of the experimental setup for parallel processing with multiplexing element and (b) the captured photograph during etching.

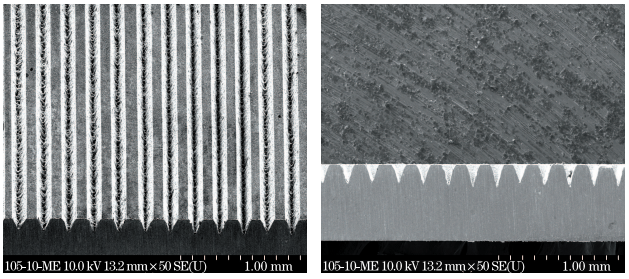

(a) (b)

Fig. 6. SEM images for (a) top view and (b) cross-sectional profile of the microgrooves produced in 10% H_3PO_4 using the parallel processing. Process conditions are P_{in}=3.5 W, P_{out} (each port)=1.25 W, V=4 μm/s, D_{core}=105 μm, and D_{gap}=90 μm.

the manufacturing throughput can be increased substantially by using multiple fibers for parallel processing.

Figures 5(a) and (b) show a simple schematic diagram of the experimental setup for parallel processing and a photograph of parallel etching using two optical fibers, respectively. For division of the laser beam, a customized 1×2 fiber-optic coupler manufactured with 105-μm-core fiber is employed as a multiplexing element with an intrinsic coupling loss of about 1.5 dB; for instance, if the laser power of 3.5 W is launched into the input optical fiber, the output power of the each port of the output optical fiber would be 1.25 W.

SEM images of the microgrooves fabricated using the parallel etching setup are shown in Fig. 6. Width and depth of the grooves produced by each output optical fiber appear uniform while the groove pitches are maintained at the same value of 200 μm. Total process time for fabrication of twenty 50-mm-long grooves took about 7 hours, reducing the manufacturing time by half compared to the single optical fiber processing. The width and depth of the microgrooves are 90 and 150 μm, respectively. This result proves that the process productivity could be improved by parallel processing with the optical fiber-based LIWE technique provided that a sufficient laser power is available.

A microhole is another key configuration together with the microgroove in the fabrication of microdevices for which the proposed LIWE may become an attractive and effective technique. Drilling of a deep hole in metals, for example, over 500-μm depth, is a challenging task if the hole diameter should be around 100 μm or less. In laser ablation drilling, unwanted thermal and mechanical effects pose serious negative effects on the geometry of a drilled hole. For example, Luft *et al.*[3] reported a constriction of the hole due to redeposition of melt on the sidewall, spallation of the bottom surface just before the formation of a through hole due to high vapor and plasma pressure inside the hole, large HAZ and mechanical load on the sidewall due to plasma absorption had been observed over wide range of pulse duration (50 ns $\sim$200 fs) and irradiance ($10^8 \sim 10^{15}$ W/cm^2) for pulse laser drilling. To control and improve the hole shape, Stephen *et al.*[15] adopted a beam shaping system in which the divergence angle of the laser beam is adjusted with a Galilean telescope. By controlling laser power and beam divergence angle, the fabrication of microholes with small taper angle (min. 1 degree) was reported. Despite the improvement of hole profile, debris could not be avoided with this technique.

In the following, it is shown that the proposed LIWE technique can be applied for a nearly straight hole drilling with process optimization. When the laser beam irradiates on the workpiece, a hole forms on the workpiece but it will develop into a tapered one if a constant gap is maintained between the fiber tip and workpiece surface as was in the groove fabrication case. In hole drilling with the proposed optical fiber-based LIWE, the key issues are to concentrate the incident laser beam into the hole and to refresh etchant inside the hole so that the thermochemical reaction may be sustained within the hole. We solved these issues by oscillating the optical fiber up and down during etching as follows. Initially, the laser beam irradiates the workpiece for one minute in order to produce a key hole near the surface by maintaining a constant gap. Once a hole begins to develop after the initial 60-s irradiation, the optical fiber is oscillated between the workpiece surface and the

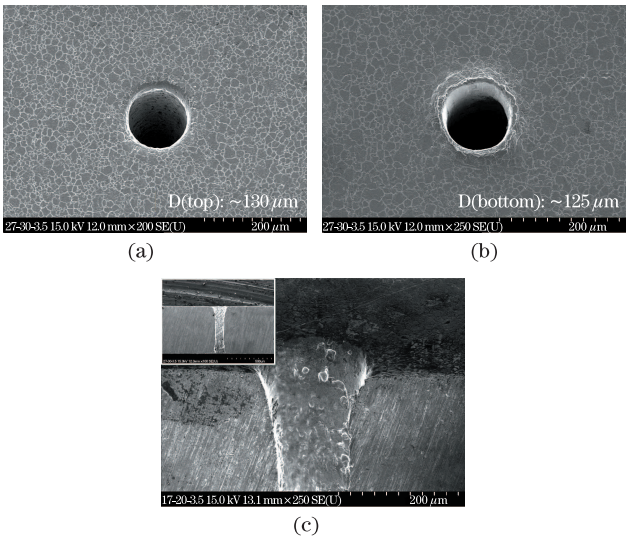

Fig. 7. SEM images for the (a) top surface view, (b) bottom surface view, and (c) magnified sidewall of the microhole fabricated on 500-μm-thick stainless steel foil in 30% H_3PO_4. Other process parameters are P=2.5→3.5 W, D_{gap}=250 μm, and D_{core}=105 μm. The inset shows the entire hole through the workpiece thickness.

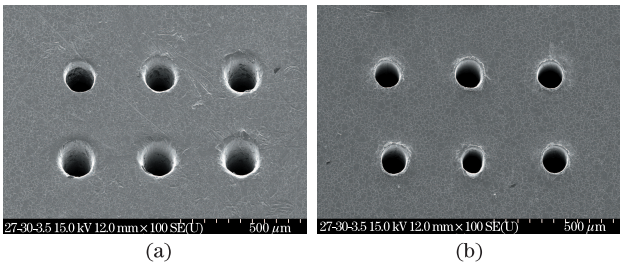

Fig. 8. SEM images for (a) top and (b) bottom view of a 3×2 microhole array fabricated on a stainless steel foil (500-μm thickness). Process conditions are P=2.5→3.5 W, C=30%, D_{gap}=250 μm, and D_{core}=105 μm.

threshold-gap height. During this oscillation period, the fiber tip dwells at the bottom position (the workpiece side) for about 0.2∼0.5 sec for irradiation in which the dwelling time depends on laser power. Similar amount of dwelling time is also provided at the top position to cool the fiber tip. As the hole depth increases, the fiber tip is inserted into the hole with a gradual increase of insertion depth. It is considered that the insertion and removal of the optical fiber into the hole helps removal of etch by-products and refreshment of etchant within the hole. This oscillating motion of the optical fiber continues until a through hole is drilled.

Figures 7(a) and (b) show the top and bottom surfaces of a drilled hole using the above described process in 30% H_3PO_4 using a 105-μm-core fiber with D_{gap}=250 μm. A relatively high etchant concentration of 30% had to be used for the hole drilling, which is most likely because the etchant becomes bleached within the closed hole when low concentration is selected. For the hole in Fig. 7, the laser power was increased from 2.5 to 3.5 W at an intermediate step due to the increase of laser energy loss and difficulty of etchant refreshment as the hole deepens. The etched hole has good circularity at both entrance and exit sides with little thermal deformation. The evaluated eccentricity ratio was around 0.048 and also total drilling time was 485 s. Figure 7(c) shows the morphology of the sidewall and the cross-sectional profile of the through hole (inset). The inner surface of the hole appears reasonably smooth although some surface microstructures are visible. The cross-section is almost straight over the entire thickness except the partially conical region near the entrance. The measured surface roughness at the machined area, R_a is below 600 nm and the aspect ratio of this hole is about 4.

Using this technique, a 3×2 microhole array is fabricated on a stainless steel foil to demonstrate reproducibility of the drilling process as shown in Fig. 8. The hole diameters at the top and bottom surfaces are about 130 and 125 μm, respectively, and the calculated taper angle is less than 1°. The six holes shown in Fig. 8 are drilled using only one optical fiber, which implies that fiber damage can be avoided if the process conditions are well adjusted even if the fiber is inserted into the hole during drilling. These results verify that the proposed LIWE technique can be effectively used in the fabrication of straight microholes with little HAZ or thermal deformation.

In conclusion, a new optical fiber-based laser micromachining is proposed to fabricate microgrooves and microholes with high-dimensional accuracy and good surface quality. Unlike other existing laser micromachining methods, the proposed technique employs an optical fiber as the machining tool. Owing to the use of optical fiber, the proposed technique has intrinsic advantages of little reflection loss of the laser beam, flexible transport of beam, no danger of potential exposure of an operator to laser light, and potential to enhance throughput by multiplexing laser beam. It is believed that the proposed LIWE could be a useful micromachining technique for the manufacture of microthermal and microfluidic devices such as micro heat pipe, micro heat spreader, micro reactor, and so on, those based on metallic microgrooves and microholes.

This work was supported by the Industrial Technology Research Infrastructure Program (No. 0000012, Infrastructure establishment on the laser processing system for the next generation micro applications) funded by the Ministry of Knowledge Economy (MKE, Korea).

References

1. B. N. Chichkov, C. Momma, S. Nolte, F. Von Alvensleben, and A. Tünnermann, Appl. Phys. A **63,** 109 (1996).
2. R. Le Harzic, N. Huot, E. Audouard, C. Jonin, P. Laporte, S. Valette, A. Fraczkiewicz, and R. Fortunier, Appl. Phys. Lett. **80,** 3886 (2002).
3. A. Luft, U. Franz, A. Emsermann, and J. Kaspar, Appl. Phys. A **63,** 93 (1996).
4. R. Nowak, S. Metev, and G. Sepold, Sensors. Actuators A **51,** 41 (1995).
5. R. Nowak and S. Metev, Appl. Phys. A **63,** 133 (1996).
6. K. H. Oh, M. K. Lee, and S. H. Jeong, J. Micromech. Microeng. **16,** 1958 (2006).
7. C. Vass, K. Osvay, and B. Hopp, Opt. Express **14,** 8354 (2006).

8. J. Wang, H. Niino, and A. Yabe, Appl. Phys. A **68,** 111 (1999).
9. S. Hasegawa, Y. Hayasaki, and N. Nishida, Opt. Lett. **31,** 1705 (2006).
10. B. W. Hussey, B. Haba, and A. Gupta, Appl. Phys. Lett. **58,** 2851 (1991).
11. A. Mora, M. Haase, T. Rabbow, and P. J. Plath, Phys. Rev. E **72,** 061604-1 (2005).
12. R. Nowak, S. Metev, and G. Sepold, Proc. SPIE **2207,** 633 (1994).
13. E. Almeida, D. Pereira, M. O. Figueiredo, V. M. M. Lobo, and M. Morcillo, Corros. Sci. **39,** 1561 (1997).
14. H. Iken, R. Basseguy, A. Guenbour, and A. Ben Bachir, Electrochim. Acta **52,** 2580 (2007).
15. A. Stephen, S. Metev, W. Jüptner, and F. Vollertsen, Proc. SPIE **6157,** 61570I (2005).